Failure Analysis of Adhesively Bonded Composite Joints

Phil Yarrington[‡], James Zhang[§] and Craig Collier[**]
Collier Research Corp., Hampton, VA 23669

Brett A. Bednarcyk[††]
University of Virginia, Charlottesville, VA 22903

Failure analysis of bonded composite joints is essential to the design of modern aerospace vehicles in which adhesive joints are widely used. Recently, methods for stress and failure analysis of composite bonded joints have been developed in a new HyperSizer® capability. The first part of the capability involves calculation of adhesive stresses, as well as detailed in-plane and out-of-plane stresses in the adherends, as described in ref. 1. This companion paper presents the second major part, which is the prediction of failure of bonded joints and validation of those predictions. Many leading bonded joint failure theories, summarized herein, were implemented, and then evaluated for accuracy against test data. Through comparison to 14 test cases with 3 different joint configurations, the ratios of predicted failure load divided by test average failure load vary from 0.77 to 0.95. These results show that HyperSizer is relatively accurate and consistent for predicting initial failure.

I.   Introduction

$\mathbf{M}$ethods for stress and failure analysis of composite bonded joints have been developed recently and implemented in a new HyperSizer® capability[1]. The capability of HyperSizer to calculate accurate three-dimensional stresses enables prediction of failure loads in bonded composite joints with complex 3D stress states. Failure prediction requires not only accurate stress analysis, but also use of appropriate failure criteria associated with specific failure modes. For bonded joints, the failure occurs either within the adhesive (cohesive failure), at the adhesive/adherend interface (interface failure), or in the adherends. Metallic adherends generally fail in relatively simple modes compared to composite adherends, which may fail in matrix tension/compression, fiber tension/compression, delamination, etc. Interfacial failure is particularly complex because of the formation of chemical bonds, whose strengths are difficult to measure. In some cases, composite joints fail progressively after damage is initiated in the adherends or in the adhesive. The ultimate failure of a joint will then not be reached until the progressively accumulated damage exceeds the tolerance. The process of damage growth is relatively complex and not easy to predict using conventional material strength methodologies. Currently, HyperSizer does not consider progressive failure, but will in the future. In this paper, a number of failure criteria are discussed for bonded joints and implemented within HyperSizer, in conjunction with the establishment of an experimental database.

[‡] Senior Research Engineer, 2 Eaton St., Suite 504, Hampton, VA 23669, AIAA Member.
[§] Research Engineer, 2 Eaton St., Suite 504, Hampton, VA 23669, AIAA Member.
[**] Senior Research Engineer, 2 Eaton St., Suite 504, Hampton, VA 23669, AIAA Senior Member.
[††] Senior Research Scientist, Department of Civil Engineering, AIAA Member.

The objective of this paper is to validate HyperSizer's failure analysis capabilities with experimental data from the literature. The first example is selected from Cheuk and Tong's experiment and analysis for lap shear joints[2]. The original purpose of the study by Cheuk and Tong was to investigate the interlaminar failure of bonded shear lap joints with embedded cracks. In this study, experiments were conducted to identify the failure modes and to measure failure loads of specimens with different crack lengths. In our present study, we select the validation cases from a group of experimental results for uncracked specimens. The comparison shows that the predicted failure location in HyperSizer matches well with experimental observation, while the predicted failure load is somewhat conservative compared to the measured ultimate failure load in the tests. The discrepancy may be due to the progressive damage involved in the experiment while the predicted failure load only accounts for the damage initiation. The second validation example is selected from composite bonded skin/stringer specimens tested by NASA[3-5]. Both linear and nonlinear adhesive properties are considered in this example. Failure criteria for delamination and matrix cracking are used to predict the damage onset and the corresponding margin of safety is checked in a point-wise manner. The predicted location of damage onset by linear analysis is consistent with the experimental observation, while the predicted load for the damage initiation is approximately 0.85 times that of the average tested strength. Nonlinear adhesive analysis shows that the compliant adhesive will significantly increase the damage resistance of the adherends. The last validation example is selected from the bonded single-lap joint specimens studied by Tong[6]. Both linear and nonlinear analyses were performed to predict the failure load of the specimen subjected to longitudinal tension. The maximum stress criterion was used to predict the initial failure of the adherends based on the failure mode observed in the tests. Even though only the ultimate failure load is reported in the paper, the load-displacement curves of the joint specimens show evidence of pronounced initial damage and damage evolution prior to the ultimate failure. The failure location predicted by HyperSizer matches with the test, and the theoretical failure load correlates well with the measured initial failure load. Table 1 summarizes the theoretical predictions of the failure loads vs. test averages for each of the three HyperSizer validation problems.

Table 1 Summary of theoretical predictions vs. test averages of failure loads

Experiment		HyperSizer with Linear Adhesive		HyperSizer with Nonlinear Adhesive	
Test Examples (all the joints are subjected to longitudinal tension)	Failure loads (kN)	Theoretical Failure Load (kN)	Ratio of the Theoretical to the Test	Theoretical Failure Load (kN)	Ratio of the Theoretical to the Test
Test Example 1 Bonded doubler by Cheuk (Average of 6 tests) Characteristic distance = 0.0	18.6	13.5	0.73	14.4	0.77
Test Example 2 Stepped bonded doubler by NASA (Average of 5 tests) Characteristic distance = ½ ply thickness	17.8	13.5	0.76	15.4	0.87
Test Example 3 Single-lap joint by Tong (Average of 3 tests) Characteristic distance = 0.0	7.2	6.85	0.95	6.82	0.95

Table 1 summarizes 14 total tests involving three different bonded joint designs, a bonded doubler, a stepped bonded doubler, and a single-lap joint, each composed of a different material. The ratios of the 14 linear predicted failure loads to the test results range from 0.73 to 0.95, with average equal to 0.84; the ratios of the 14 nonlinear predicted failure loads to the test results range from 0.77 to 0.95, with average equal to 0.86 (refer to Tables 3, 6, and 7).

II.   Description of HyperSizer Method

HyperSizer's stress analysis method was developed based upon Mortensen's unified approach[7], but it has been extended considerably and modified to enable accommodation of transverse in-plane straining and hygrothermal loads, and, most importantly, to compute the local in-plane and interlaminar stresses throughout the adherends. Compared to other analytical methods used for bonded joint analysis, the HyperSizer method is capable of handling more general situations, including various joint geometries, both linear and nonlinear adhesive behavior, asymmetric and unbalanced laminates, and more general loading and boundary conditions. A wide range of joint types may be considered in HyperSizer, and the adherends, which were originally modeled as classical laminates in cylindrical bending, are now considered to undergo 'generalized cylindrical bending', in which transverse straining is accommodated. Both linear and nonlinear behavior of the adhesive layer is admitted in the analysis. For linear analysis, the adhesive layer is modeled as continuously distributed linear tension/compression and shear springs. Inclusion of nonlinear adhesive behavior in the analysis is accomplished through the use of a secant modulus approach for the nonlinear tensile stress–strain relationship in conjunction with a yield criterion. Finally, the equilibrium equations for each joint are derived, and by combination of these equations and relations, a set of governing ordinary differential equations is obtained. The governing system of equations is solved numerically using Mortensen's 'multi-segment method of integration,' yielding laminate-level fields and adhesive stresses that vary along the joint in each adherend. After the governing equations are solved, the ply-level in-plane stress components in the adherends can be calculated from Classical Lamination Theory (CLT). After solving for the in-plane stresses, the interlaminar stress components of adherends are obtained through integration of point-wise equilibrium equations. The details of HyperSizer stress analysis method is described in ref. 1. It is worthy of mentioning that HyperSizer program is very efficient; the execution time for a typical bonded doubler problem is approximately 1/40 second, enabling rapid consideration of a wide range of joint configurations for sizing optimization.

III.   Failure Criteria for Composite Bonded Joints

Failure analysis was performed using the stress analysis results together with a set of strength-based failure criteria corresponding to specific failure modes of composite bonded joints. These failure modes fall into two broad categories, as shown in Fig.1; those that apply to the adherends, such as matrix or fiber cracking or delamination, and those that apply to the adhesive. The failure criteria are described below.

A. Composite adherend failure

General failure criteria for laminated adherends

The failure modes for the adherends made of composite laminates are the same as those of stand-alone laminates, which experience either matrix failure or fiber failure. A number of failure criteria have been proposed for each failure mode using either phenomenological models or micromechanics approaches. For example, Hashin[8-9] has proposed a set of 2D failure criteria for unidirectional laminates based on failure modes of the individual plies within the laminate:

Tensile fiber mode ($\sigma_1 > 0$)

$$\left(\frac{\sigma_1}{X_T}\right)^2 + \left(\frac{\tau_{12}}{S}\right)^2 = 1 \tag{1}$$

Compressive fiber mode ($\sigma_1 < 0$)

$$\left|\sigma_1\right| = X_C \tag{2}$$

Tensile matrix mode ($\sigma_2 > 0$)

$$\left(\frac{\sigma_2}{Y_T}\right)^2 + \left(\frac{\tau_{12}}{S}\right)^2 = 1 \tag{3}$$

Compressive matrix mode ($\sigma_2 < 0$)

$$\left(\frac{\sigma_2}{2S_T}\right)^2 + \left[\left(\frac{Y_C}{2S_T}\right)^2 - 1\right]\frac{\sigma_2}{Y_C} + \left(\frac{\sigma_{12}}{S}\right)^2 = 1 \tag{4}$$

where σ_1, σ_2, and τ_{12} are the ply longitudinal, transverse, and shear stress components in the ply principal material coordinate system, X_T and X_C are the ply longitudinal tensile and compressive strengths, Y_T and Y_C are the ply transverse tensile and compressive strengths, S is the ply in-plane shear strength, and S_T is the ply out-of-plane transverse shear strength.

Hashin's failure theory has been continuously improved and extended by many researchers, such as Sun and Tau[10], Puck et al.[11], and Davila and Comanho[12], among others.
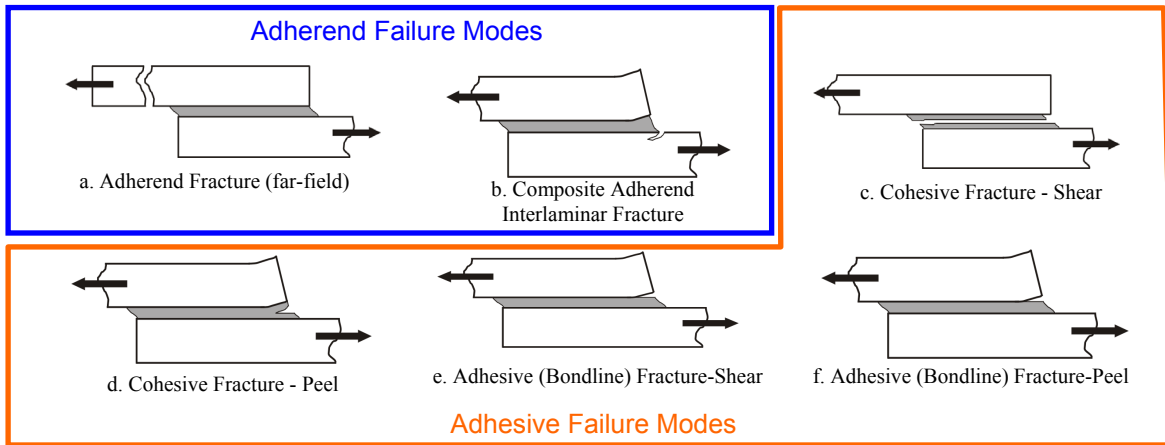

Fig.1 Failure modes in adhesively bonded joints identified by Heslehurst and Hart-Smith[13].

Composite Adherend Interlaminar Fracture (Delamination)

Interlaminar delamination is a typical failure mode for composite bonded joints due to the weakness of composite adherends subjected to interlaminar shear and transverse normal peel stresses. There are a number of failure criteria for this failure mode.

American Institute of Aeronautics and Astronautics

Adams and Wake[14] proposed a simple maximum stress criterion, which assumed that interlaminar failure in a composite adherend occurs when the normal tensile stress at the interface exceeds its ultimate strength. It is given as

$$\frac{\sigma_3}{Z} = 1 \tag{5}$$

where σ_3 is the ply interlaminar normal stress and Z is the through-thickness tensile strength of the composite plies. This criterion regards the interfacial peel stress is the major contributor to the delamination failure.

Hoyt et al.[15] adopted the following failure criterion to predict the damage initiation induced by interlaminar stresses in skin/flange specimens with $[45°/0°/45°/0°/45°/0°/45°/0°/45°]$ IM7/8552 fabric for the flange and $[45°/-45°/90°/45°/-45°/0°/-45°/45°/90°/-45°/45°]$ graphite/epoxy prepreg tape for the skin. The criterion is given as

$$\frac{\sigma_3}{Z} + \left(\frac{\tau_{13}}{R}\right)^2 = 1 \tag{6}$$

where τ_{13} is the ply interlaminar shear stress and R is the through-thickness shear strength of the plies in the laminated adherends. In general, the ply normal tensile strength is less than the through-thickness shear strength, so in Eq. (6), the contribution from the normal stress to the laminate failure is greater than the shear stress. Thus this criterion can be regarded as matrix-dominated interfacial criteria. This criterion has been examined by Long[16], who concluded that the observed failures within the prepreg layer can be accurately described using Eq. (6) for adhesively bonded ARALL-1 single and double-lap joints. However, Tong[17] found that it is less accurate as fiber breakage becomes involved along with interlaminar delamination within the 0-degree surface ply near the bondline. Thus, Tong proposed and tested six failure criteria considering the contribution of axial stresses to delamination combined with fiber breakage. Those failure criteria are given as

$$\frac{\sigma_1(\sigma_1 - \sigma_3)}{X_T^2} + \left(\frac{\sigma_3}{Z}\right)^2 + \left(\frac{\tau_{13}}{R}\right)^2 = 1 \tag{7}$$

$$\frac{\sigma_1(\sigma_1 - \sigma_3)}{X_T^2} + \left(\frac{\sigma_3}{Z}\right) + \left(\frac{\tau_{13}}{R}\right)^2 = 1 \tag{8}$$

$$\left(\frac{\sigma_1}{X_T}\right)^2 + \left(\frac{\sigma_3}{Z}\right)^2 + \left(\frac{\tau_{13}}{R}\right)^2 = 1 \tag{9}$$

$$\left(\frac{\sigma_1}{X_T}\right)^2 + \left(\frac{\sigma_3}{Z}\right) + \left(\frac{\tau_{13}}{R}\right)^2 = 1 \tag{10}$$

$$\frac{\sigma_1(\sigma_1 - \sigma_3)}{X_T X_C} + \left(\frac{\sigma_3}{Z}\right)^2 + \left(\frac{\tau_{13}}{R}\right)^2 = 1 \tag{11}$$

$$\frac{\sigma_1(\sigma_1 - \sigma_3)}{X_T X_C} + \left(\frac{\sigma_3}{Z}\right) + \left(\frac{\tau_{13}}{R}\right)^2 = 1 \tag{12}$$

A 3-D extension to Eq. (7) that accounts for transverse normal and in-plane shear stress has also been implemented. This equation is given as:

$$\left(\frac{\sigma_1^2 - \sigma_1 \sigma_3}{X_T X_C}\right) + \left(\frac{\sigma_2^2 - \sigma_2 \sigma_3}{Y_T Y_C}\right) + \left(\frac{\sigma_3}{Z}\right)^2 + \left(\frac{\tau_{23}}{Q}\right)^2 + \left(\frac{\tau_{13}}{R}\right)^2 + \left(\frac{\tau_{12}}{S}\right)^2 = 1 \tag{13}$$

In addition, Camanho and Matthews[18] proposed two quadratic-form failure criteria for onset of delamination based on Hashin work. They are given as

$$\left(\frac{\sigma_3}{Z}\right)^2 + \left(\frac{\tau_{23}}{Q}\right)^2 + \left(\frac{\tau_{13}}{R}\right)^2 = 1, \quad \sigma_3 > 0 \tag{14}$$

and

$$\left(\frac{\tau_{23}}{Q}\right)^2 + \left(\frac{\tau_{13}}{R}\right)^2 = 1, \quad \sigma_3 < 0 \tag{15}$$

where Q is transverse shear strength of the ply.

Matrix cracking

In addition to delamination in the adherends, matrix cracking is also considered as a major damage mode in laminated adherends. Minguet and co-workers[19-22] investigated composite skin-stiffener debonding and believed that the maximum tensile stress in the matrix leads to matrix cracking. Thus, the corresponding failure criterion is given as

$$\frac{\sigma_{tt\_p}}{Y_T} = 1 \tag{16}$$

where σ_{tt_p} is the maximum principal stress in the transverse plane, given by $\sigma_{tt\_p} = \frac{\sigma_2 + \sigma_3}{2} + \sqrt{(\frac{\sigma_2 - \sigma_3}{2})^2 + \tau_{23}^2}$.

Adherend fracture

Adherend fracture (sectional failure) is also a common failure mode in composite bonded joints. Cheuk et al.[2] reported this type of failure in a series of experiments on bonded doublers made of T300/934 plain woven prepreg laminates. In general, maximum stress or strain criteria can describe this type of failure. The maximum stress can be the maximum ply-level principal stress or the maximum in-plane stress. The general form of the failure criterion can be given as

$$\frac{\sigma^{max}}{X_T} = 1 \quad \text{or} \quad \frac{\varepsilon^{max}}{e_t^{ult}} = 1 \tag{17}$$

where e_t^{ult} is the ultimate tensile strains and σ^{max} and ε^{max} are the maximum tensile strain and maximum tensile stress for any adherend ply.

B. Adhesive Failure (cohesive and adhesive/adherend interface failure)

Adhesives are more susceptible to failure due to tensile strain than pure shear and compression. For some adhesives, nonlinear behavior dominates and strain to failure can exceed 100%. Thus, for the cohesive failure of ductile adhesives, the maximum strain criterion is usually applied. It is given as

$$\frac{\varepsilon_{eqv.}}{S_{eqv.}} = 1 \tag{18}$$

where $\varepsilon_{eqv.}$ is the von Mises equivalent strain and $S_{eqv.}$ is the failure strain[15].

Failure of the spew fillet is another special case needed to be considered for adhesive failure. Adams and Harris[23] have studied the failure mechanism in adhesive spew fillets, and found that initial damage in the spew fillet is caused by the tensile stress. As a result, the maximum principal stress criterion is applied to this type of failure. It is given as

$$\frac{\sigma_p^{max}}{X_T} = 1 \tag{19}$$

where σ_p^{max} is the max principal stress and X_T is the tensile strength of bulk adhesive.

The adhesive failure is also sometimes referred to as bondline failure, which contains either decohesion or debonding of the interface, or mix of both. For the bondline failure, the failure mechanisms are rather complicated because these two failure mechanisms are usually mixed together in the actual failure, and the strengths of the bondline for each type of failure mechanism are different and difficult to measure, especially the strength of the adhesive/adherends interface. Thus, some engineering failure criteria have been proposed to combine these two failure mechanisms together, in which case the strengths for these two failure mechanisms are not distinguished. The following are the bondline failure criteria, which have been used by Tong and Steven[27]:

$$\left(\frac{\sigma_{zz}}{F_{peel}}\right)^2 + \left(\frac{\tau_{xz}}{F_{shear}}\right)^2 + \left(\frac{\tau_{yz}}{F_{shear}}\right)^2 = 1 \qquad \sigma_{zz} > 0 \tag{20}$$

$$\left(\frac{\tau_{xz}}{F_{shear}}\right)^2 + \left(\frac{\tau_{yz}}{F_{shear}}\right)^2 = 1 \qquad \sigma_{zz} < 0 \tag{21}$$

where σ_{zz}, τ_{xz}, and τ_{yz} are the peel and shear stresses in the adhesive and F_{peel} and F_{shear} are the bondline peel and shear strengths, which can be backed out from the above failure criteria by using the failure stresses measured in tensile shear experiments.

For shear dominated bondline failure, the contribution of peel stress is excluded from the failure criteria Eq. (20) and (21). The failure criterion can then be written as,

$$\left(\frac{\sqrt{\tau_{xz}^2 + \tau_{yz}^2}}{F_{shear}} \right) = 1 \tag{22}$$

Likewise, for peel dominant bondline failure, the contribution of shear stresses is excluded from the failure criteria Eq. (20) and (21). The failure criterion can then be written as,

$$\left(\frac{\sigma_{zz}}{F_{peel}} \right) = 1 \tag{23}$$

C. Fracture Mechanics Based Failure Criteria

The methods presented so far have dealt primarily with damage initiation, rather than with ultimate failure, which is much more difficult to predict. In order to predict ultimate failure, implementation of a fracture mechanics based failure criteria is currently being pursued. This approach recognizes that all materials contain flaws and that adhesive joints usually fail by the initiation (or sub critical growth) and propagation of flaws of a critical size within the adhesive layer or composite adherends. Fracture mechanics attempts to link these processes with predictions of the joint strength under various loading conditions by analyzing the stress state within the joint, particularly in the vicinity of the critical flaw and comparing this with material properties that describe the tendency of the cracks to propagate. Results related to fracture mechanics based failure criteria will be presented in future work.

D. Characteristic Distance

Typical joint configurations, such as single lap joints, contain bimaterial interface corners or free edges that can result in theoretically singular stress/strain fields. In these circumstances the failure criteria involving maximum stress/strain are meaningless. However, Adams Peppiatt[24] insisted that sharp corners do not exist in real joints and therefore neither do the stress/strain singularities. This is a valid point, but as observed by Adams and Harris[23], the predicted values of the maximum stress/strain components are highly sensitive to small changes of the local joint geometry at the leading edges, whereas the experimental results are not. Thus, although reasonable success has been obtained with maximum stress/strain failure criteria, there is analytical and experimental evidence to suggest that this form of failure criteria is only suitable for adhesive joints when some averaged value is used. This leads directly into the concept of characteristic distance.

A way of getting around the problems associated with maximum stress/strain criteria is to use a maximum stress/strain at a given distance from the point of singularity or a critical value of stress/strain averaged over a given region. This distance is the so-called characteristic distance. This is, in effect, what has been implemented with most of the criteria that were evaluated using closed-form type solutions and FEA. The stress/strain has either been found at a certain fixed distance from the singularity, or some averaged value has been used.

IV. Validation Examples

A. Bonded Doubler Validation – Cheuk Example

This example is selected from Cheuk and Tong's[2] failure tests on bonded doublers. For convenience, we refer to it as Cheuk's problem. Fig. 2 depicts schematically the geometric configuration of bonded doubler specimens used by Cheuk and Tong. The specimens have an overlap length of 45 mm and an unsupported length of 95 mm. The material used for manufacturing the composite adherends was T300/934 carbon/epoxy plain-woven, with orientation of 0°. In HyperSizer failure analysis, both linear and nonlinear adhesive were used to predict the failure load of the specimen subjected to longitudinal

tension. Tables 2a and 2b provide the material properties of the adherend plies and the adhesive. Note that S_{prop} is the proportional limit of adhesive, and S_{ult} and e_{ult} are the ultimate stress and strain, respectively. λ is the ratio of compressive yield stress to the tensile yield stress of the adhesive. Figure 3 plots the experimental stress-strain data for FM300-K along with the employed non-linear approximation using the Ramberg-Osgood model.

The stress analysis results for the in-plane stress of the surface ply and out-of-plane stresses of the adherends at the free edge are shown in Figs. 4 and 5. The maximum principal stress criterion, i.e. Eq. (17) is used to predict the sectional fracture of the adherends because it is believed that the sectional fracture is caused by the maximum tensile stress in the adherends. The margin of safety is checked at every point of the adherends, including at the free edges, as shown in Figs. 6 and 7. The predicted failure loads are summarized in Table 3, together with the comparison to test results.
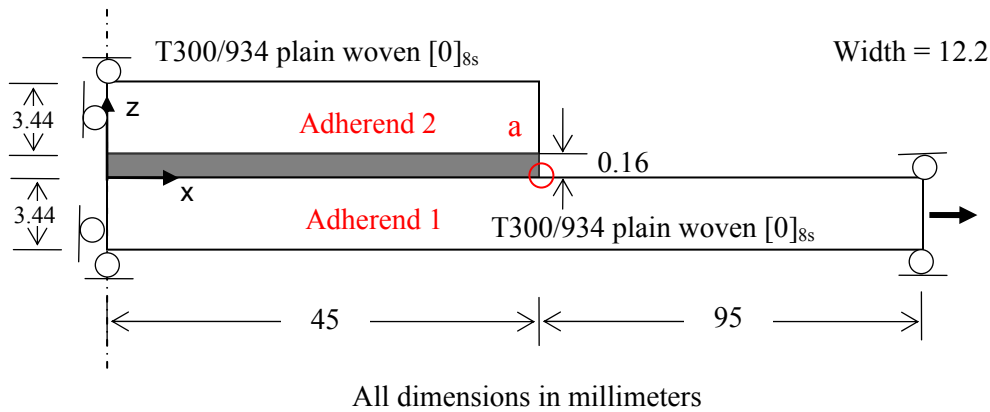

All dimensions in millimeters

Fig. 2 Schematics of bonded doubler specimen studied by Cheuk and Tong[2].

Table 2a Properties of a ply of T300/934 carbon/epoxy plain woven prepreg

Longitudinal modulus $E_1 = E_2$, MPa	57226
Transverse modulus E_3, MPa	4800
In-plane shear modulus G_{12}, MPa	4481
Out-of-plane shear modulus $G_{13} = G_{23}$, MPa	4400
In-plane Poisson ratio v_{12}	0.05
Out-of-plane Poisson ratio $v_{13} = v_{23}$	0.28
In-plane tensile strength X_t, MPa	518

Table 2b Mechanical properties of FM300-K adhesive

	E (GPa)	v	S_{prop} (MPa)	S_{ult} (MPa)	e_{ult}	λ
FM300-K	2.40	0.32	25.92	69.88	0.0685	1.0

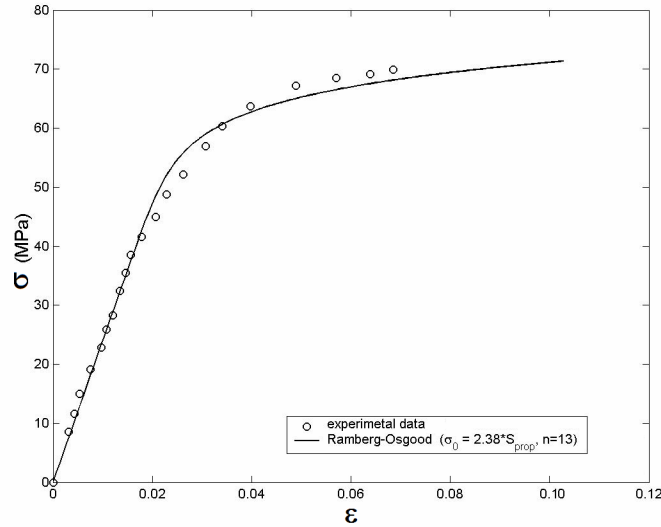American Institute of Aeronautics and Astronautics

Fig. 3 Experimental nonlinear stress-strain data for FM300-K adhesive along with Ramberg-Osgood approximation.

Table 3 Summary of theoretical failure load vs. experimental result of Cheuk example (CD[1] = 0, failure criterion = Eq. (17), failure mode = sectional fracture)

Experiment		HyperSizer Theoretical			
		Linear Adhesive		Nonlinear Adhesive	
Number	Final Failure Load (kN)	Theoretical Failure Load (kN)	Ratio of the Theoretical to the Test	Theoretical Failure Load (kN)	Ratio of the Theoretical to the Test
1	19.162	13.5	0.70	14.4	0.75
2	18.272	13.5	0.74	14.4	0.79
3	17.502	13.5	0.77	14.4	0.83
4	18.987	13.5	0.71	14.4	0.76
5	18.765	13.5	0.72	14.4	0.77
6	19.048	13.5	0.71	14.4	0.76
Average	18.623	13.5	0.73	14.4	0.77

1. CD stands for characteristic distance

B. Bonded Doubler Validation – NASA Example

The next validation example involves skin/flange specimens which were studied by NASA[3], as shown schematically in Fig. 8. The specimen consists of a tapered flange bonded to the skin. The skin was made of IM7/8552 graphite/epoxy prepreg tape and had a nominal ply thickness of 0.148 mm and a [45°/-45°/0°/-45°/45°/90°/90°/-45°/45°/0°/45°/-45°] lay-up. The flange was made of an IM7/8552 plain woven fabric, with a lay-up of [45°/0°/45°/0°/45°/0°/45 °/0°/45°] and nominal thickness of 0.212 mm. The flange was pre-cured, cut to size, machined with a 25° taper along the edges and co-bonded with uncured skin using one ply of grade 5, FM 300 adhesive film. The panel then was cut into 25.4 mm wide by 177.8 mm long specimens. The thickness of the adhesive layer is 0.178 mm. The adherend material properties used in the analysis are summarized in Table 4a, while the strength values employed for the skin ply material (IM7/8552 graphite/epoxy prepreg tape) are given in Table 4b. Table 4c provides the adhesive properties. Figure 9 provides a plot of the nonlinear adhesive Ramberg-Osgood representation employed in the model vs. experimental stress-strain data.
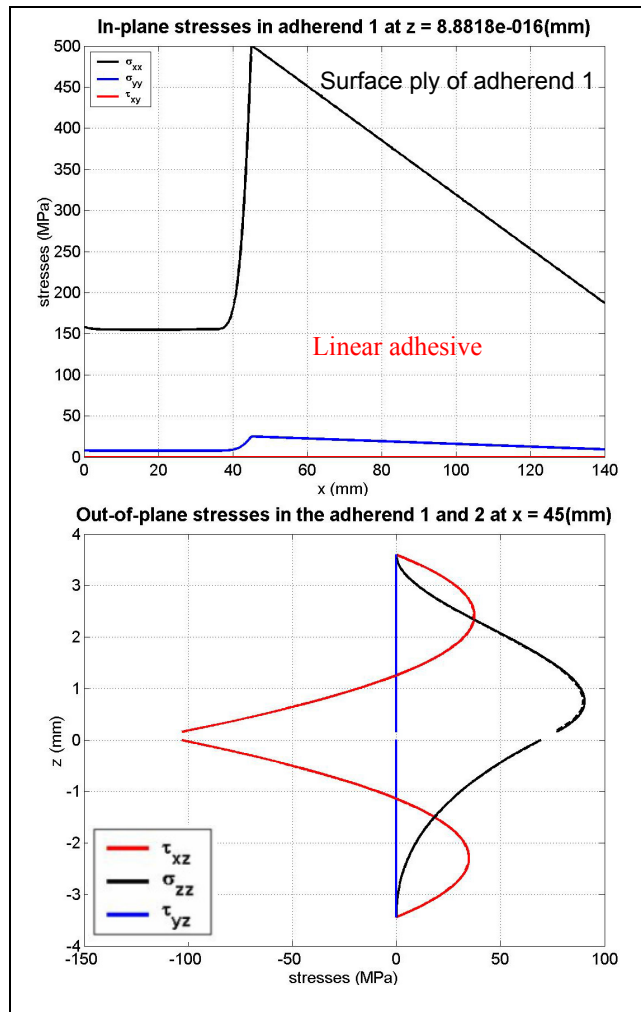
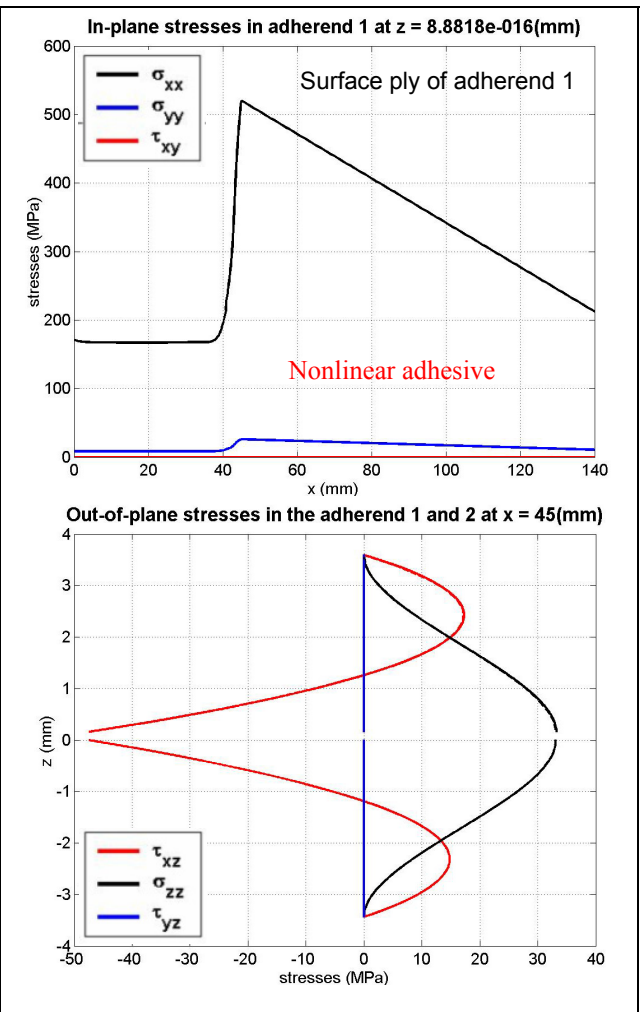**Fig. 4 Stresses in the adherends with <u>linear</u> adhesive under P =13.5 kN.**

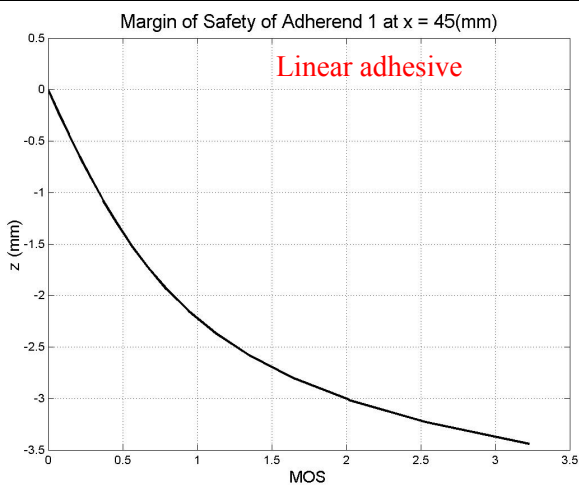**Fig. 5 Stresses in the adherends with <u>nonlinear</u> adhesive under P =14.4 kN.**

Fig. 6 Through-the-thickness margin of safety of adherend 1 at point *a* with <u>linear</u> adhesive under P =13.5 kN.
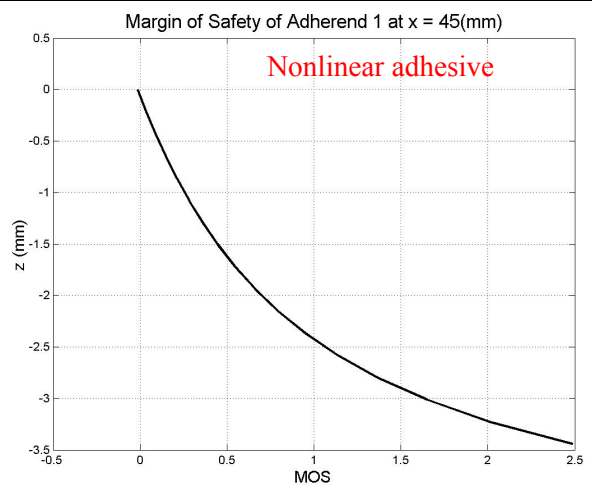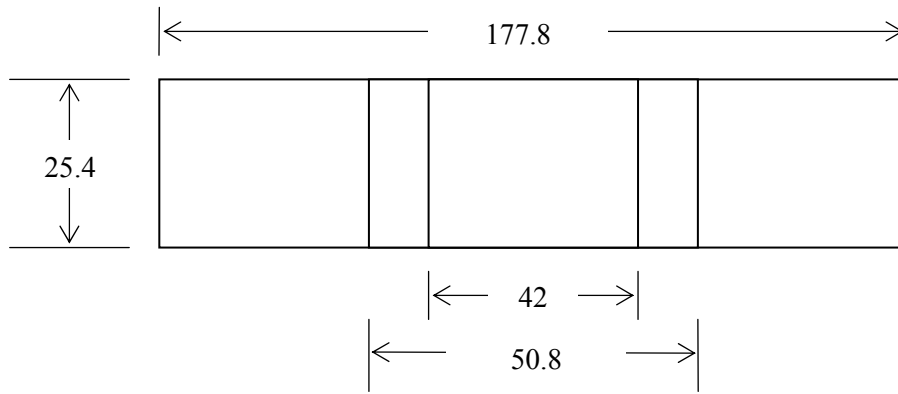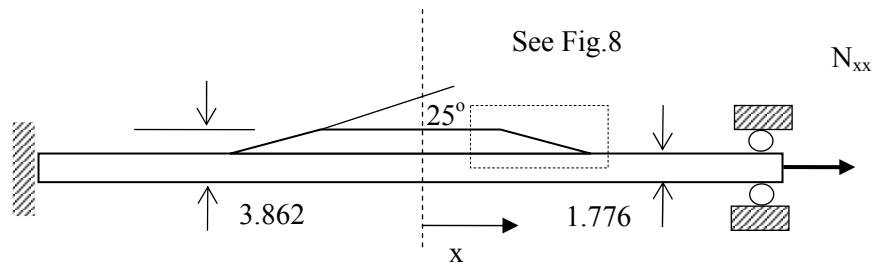

Fig. 7 Through-the-thickness margin of safety of adherend 1 at point *a* with <u>nonlinear</u> adhesive under P =14.4 kN.

11
American Institute of Aeronautics and Astronautics

All dimensions in mm

Skin: [45/-45/0/-45/45/90/90/-45/45/0/45/-45] IM7/8552 Prepreg, t_{ply} = 0.148 mm
Stiffener: [45/0/45/0/45/0/45/0/45] IM7/8552 plain woven fabric, t_{ply} = 0.212 mm
Adhesive: Grade 5 FM300, thickness = 0. 178 mm

Fig. 8 Schematics of a skin/flange specimen studied by NASA[3].

Table 4a Material properties of adherends

	IM7/8552 Graphite /Epoxy Prepreg (skin)	IM7/8552 Plain Woven Fabric (flange)
E_1 (GPa)	161.0	71.7
E_2 (GPa)	11.38	71.7
E_3 (GPa)	11.38	10.3
v_{12}	0.32	0.04
v_{13}	0.32	0.35
v_{23}	0.45	0.35
G_{12} (GPa)	5.17	4.48
G_{13} (GPa)	5.17	4.14
G_{23} (GPa)	3.92	4.14

Table 4b Strengths of IM7/8552 graphite /epoxy prepreg plies.

X_t (MPa)	Y_t (MPa)	X_c (MPa)	Y_c (MPa)	Z (MPa)	S (MPa)	R (MPa)	Q (MPa)
2647	127	1761	347	56.3	120	102	36.7

Table 4c Mechanical properties of Grade 5 FM300 adhesive

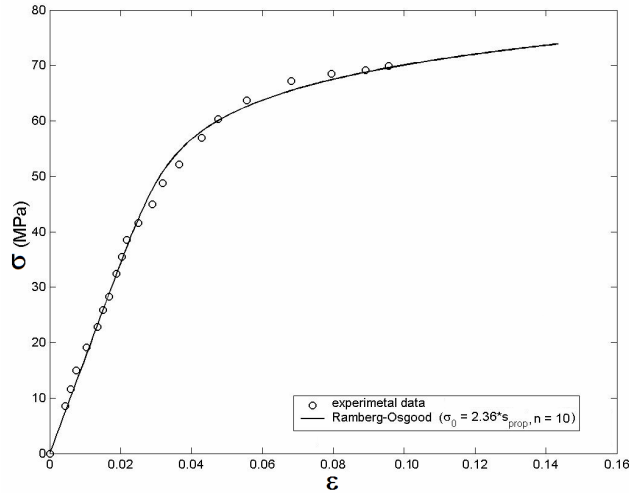|	E (GPa)	v	S_{prop} (MPa)	S_{ult} (MPa)	e_{ult}	λ
FM 300k	1.72	0.30	25.92	69.88	0.0956	1.0

Fig. 9 Experimental nonlinear stress-strain data for Grade 5 FM300 adhesive along with Ramberg-Osgood approximation.
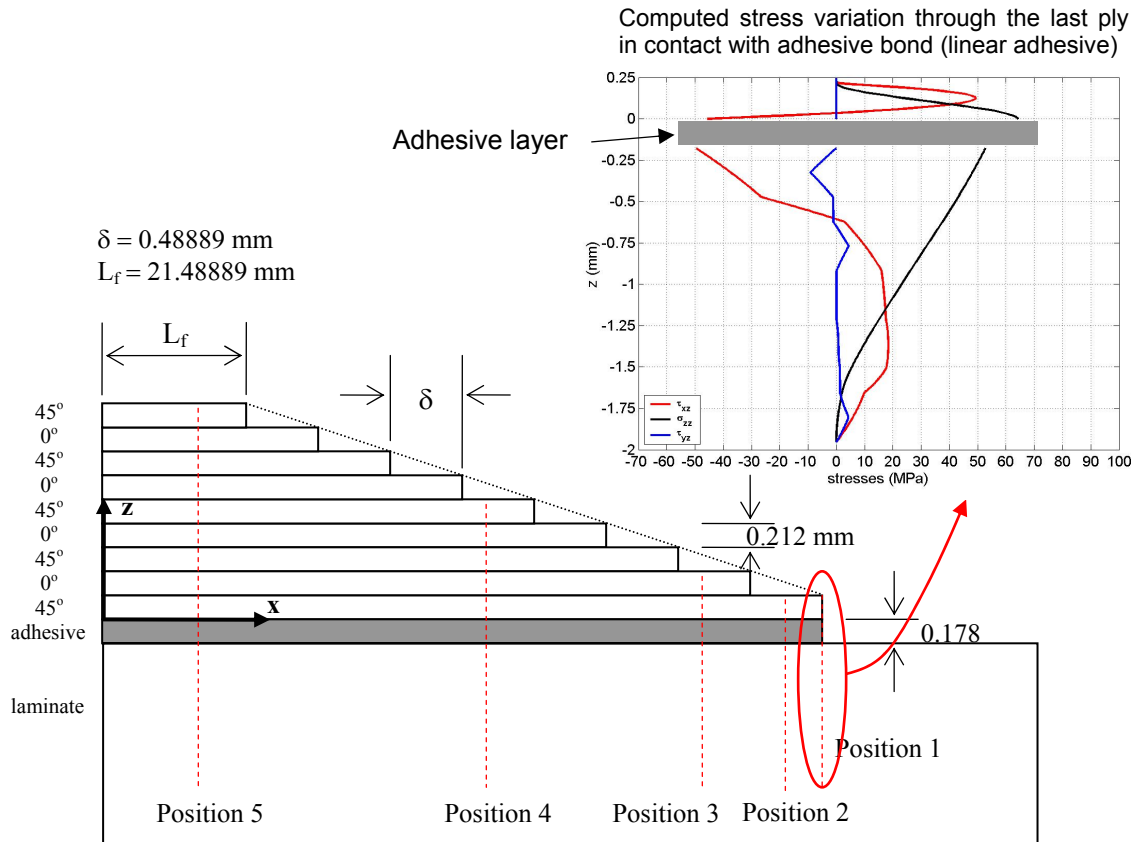

Fig. 10 Modeling of the flange scarf and interlaminar stresses at the leading edge.

The tapered ends of the flange were modeled as stepped ends in HyperSizer, as shown in Fig. 10. The joint displacements, internal forces/moments as well as local stresses are calculated in the solution domain shown in Fig. 10, which is half of the actual specimen configuration due to symmetry. Figure 10 also shows the detailed through-thickness distribution of the out-of-plane stresses at the adherend leading edge, assuming linear adhesive behavior. The interlaminar stresses distributions through the thickness of adherends are plotted at several locations near the adherend leading edges, as shown in Fig. 11, again assuming linear adhesive behavior.

Both linear and nonlinear adhesives were used in the stress analysis. The stress analysis results provided the basis for failure analysis. The failure criteria for delamination (Eqs. (5)-(15)) and matrix cracking (Eq. (16)) were used to predict the onset of damage. The corresponding margins of safety were checked at each point of the skin adherend. The failure load was then determined from the failure criterion that gives the lowest margin of safety. Because failure of the test specimens was observed in the skin adherend only[3], failure criteria were not checked for the tapered flange. Table 5 summarizes the predicted initial failure loads and failure criteria used in HyperSizer for the NASA problem. A characteristic distance of one-half ply thickness was used in predicting the failure loads. Tables 6a and 6b compare predictions based on the controlling failure mode (delamination) for linear and nonlinear adhesive analyses and characteristic distances of 0 (Table 6a) and ½ ply thickness (Table 6b).

Table 5 Predicted failure loads and failure criteria used in HyperSizer for NASA problem (Note the theoretical average delamination load =17.7 kN, very close to the test average 17.8 kN)

Failure Mode & Failure criteria	Predicted Failure Loads (kN)	
	$CD^1 = 0$	$CD = ½\ t_{ply}$
Adherend fracture, Eq. (16)	23.6*	25.1*
Adherend fracture, Eq. (17)	69.4*	70.6*
Adherend delamination, Eq. (5)	19.0	20.0
Adherend delamination, Eq. (6)	18.0	18.9
Adherend delamination, Eq. (15)	17.3	18.1
Adherend delamination, Eq. (7)	17.5	18.3
Adherend delamination, Eq. (8)	16.5	17.2
Adherend delamination, Eq. (9)	17.5	18.3
Adherend delamination, Eq. (10)	16.4	17.2
Adherend delamination, Eq. (11)	19.0	20.0
Adherend delamination, Eq. (12)	18.9	20.0
Adherend delamination, Eq. (14)	12.4	13.6
Adherend delamination, Eq. (13)	12.3	13.5
Average of delamination loads	16.8	17.7

1. CD stands for characteristic distance.   *   Excluded from the average.
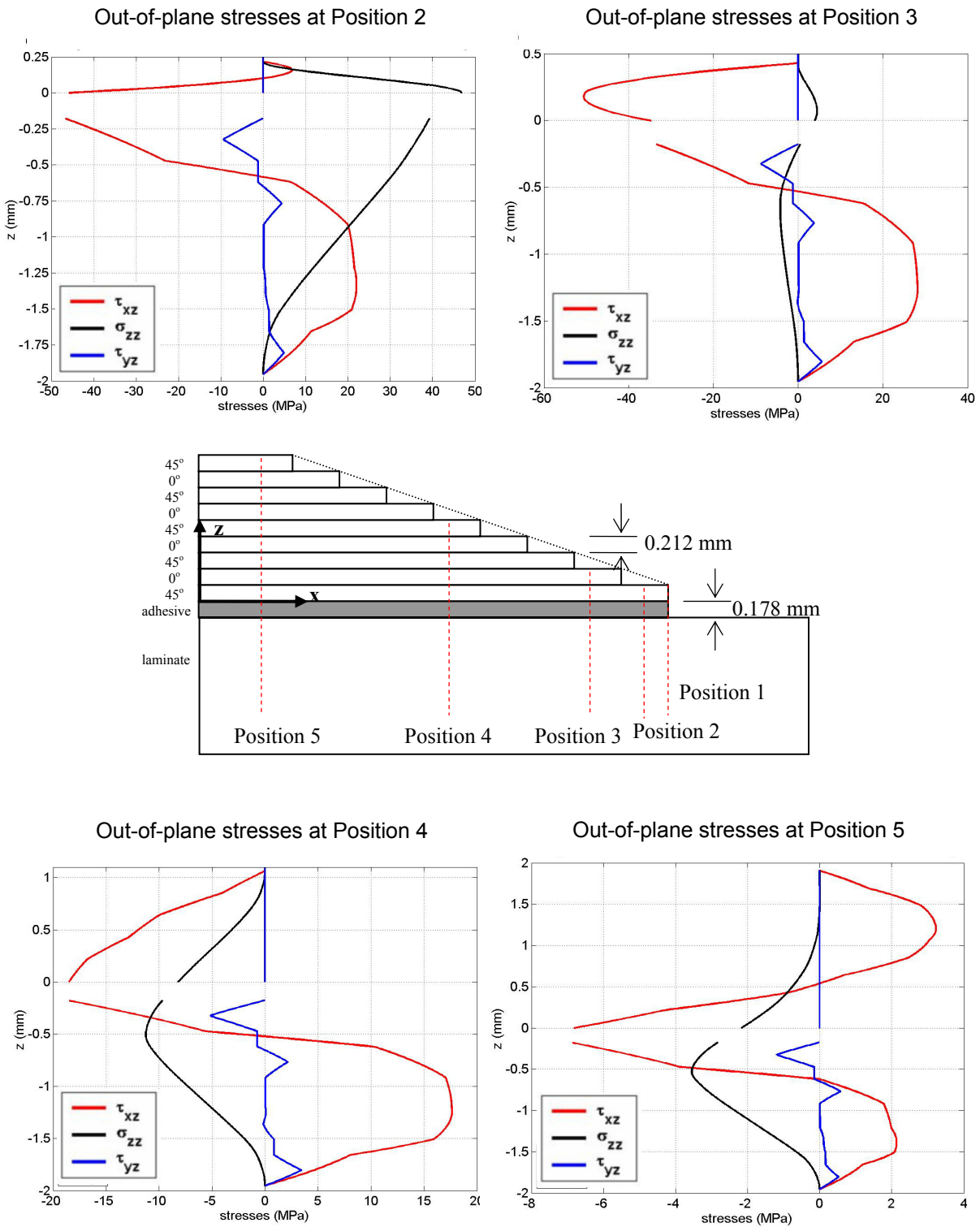
Fig. 11 Through-the-thickness distribution of interlaminar stresses at positions 2, 3, 4 and 5, as shown in Fig. 8 (linear adhesive).

Table 6a Summary of theoretical initial failure load vs. experimental result of NASA problem (CD[1] = 0, failure criterion = Eq. (13), failure mode = delamination)

Experiment		HyperSizer Theoretical			
		Linear Adhesive		Nonlinear Adhesive	
Number	Initial Failure Load[2] (kN)	Theoretical Failure Load (kN)	Ratio of the Theoretical to the Test	Theoretical Failure Load (kN)	Ratio of the Theoretical to the Test
1	16.2	12.3	0.76	13.9	0.86
2	16.5	12.3	0.75	13.9	0.84
3	18.1	12.3	0.68	13.9	0.77
4	18.3	12.3	0.67	13.9	0.76
5	19.8	12.3	0.62	13.9	0.70
Average	17.8	12.3	0.69	13.9	0.78

Table 6b Summary of theoretical initial failure load v.s experimental result of NASA problem (CD[1] = ½ t_{ply}, failure criterion = Eq. (13), failure mode = delamination)

Experiment		HyperSizer Theoretical			
		Linear Adhesive		Nonlinear Adhesive	
Number	Initial Failure Load[2] (kN)	Theoretical Failure Load (kN)	Ratio of the Theoretical to the Test	Theoretical Failure Load (kN)	Ratio of the Theoretical to the Test
1	16.2	13.5	0.83	15.4	0.95
2	16.5	13.5	0.82	15.4	0.93
3	18.1	13.5	0.75	15.4	0.85
4	18.3	13.5	0.74	15.4	0.84
5	19.8	13.5	0.68	15.4	0.78
Average	17.8	13.5	0.76	15.4	0.87

1. CD stands for characteristic distance.
2. Only initial failure loads were reported by NASA.

C. Single Lap Joint Validation – Tong[6] Example

Tong's example of single-lap joint specimens without pre-cracks was selected as another validation example for single-lap joints. The specimen configuration is schematically illustrated in Fig. 12. The joint has an overlap length of 50 mm and a nonoverlap length of 100 mm for both adherends, which are manufactured by laminating eight plies of T300/934 plain woven prepreg, oriented in the 0° direction. The adherends were bonded together using FM300-K film adhesive with uniform thickness of 0.16 mm. Material properties for these materials are given in Tables 2a and 2b. Both linear and nonlinear analyses were performed to predict the failure load of the specimen subjected to longitudinal tension. Figures 13 and 14 show the in-plane stresses in the surface ply of adherend 1 for the linear and nonlinear adhesive cases. The maximum stress criterion, Eq. (17), is used to predict initial failure of the adherends. The margin of safety is checked in the adherends, as shown in the Figs. 13 and 14. The experimental load-displacement curves of the joint specimens show very pronounced initial damage and damage evolution prior to the ultimate failure. The failure location predicted by HyperSizer, which corresponds to the location of zero margin of safety in Figs. 13a and 14a, matches well with the experimental observation (see circled locations in Fig. 12). The predicted failure load with linear analysis is 6.85 kN, which correlates well with the measured initial failure load of 7.2 kN. The predicted initial failure load using

nonlinear adhesive is only slightly different, at 6.82 kN. This is due to the in-plane tensile stress being less affected by yield of the adhesive layer than the out-of-plane stresses. Table 7 summarizes the predicted failure loads by HyperSizer and the test results.

   Note that the original experiment tested 4 groups of specimens and each group contains precracks of different length and locations. It was found that all 4 groups with total 18 tests exhibit nearly same damage initiation mode and load. Even though the test results in Table 7 were selected from the specimens in Group A which contains no precracks, the initial failure load of 7.2 kN was the average measured from load-displacement curves of all 4 groups of specimens.
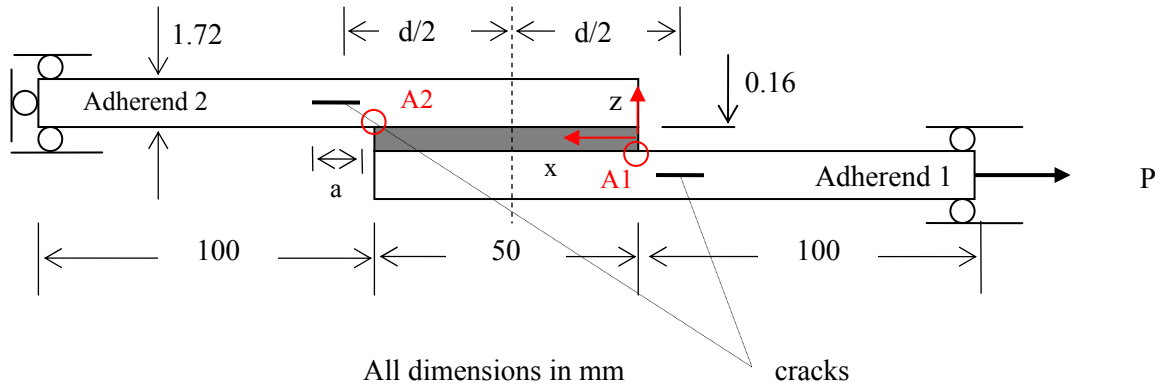

Fig. 10 The of single-lap joint problem studied by Tong[6]. Note that the uncracked case was employed for comparison herein,

Table 7 Summary of theoretical failure loads vs. experimental result of Tong example (CD[1] = 0.0, failure criteria = Eq. (17), failure mode = sectional fracture)

	Experiment		HyperSizer Theoretical			
			Linear Adhesive		Nonlinear Adhesive	
Number	Final Failure Load (kN)	Initial Failure Load (kN)	Theoretical Failure Load (kN)	Ratio of the Theoretical to the Test[2]	Theoretical Failure Load (kN)	Ratio of the Theoretical to The Test[2]
1	14.374	7.2	6.85	0.95	6.82	0.95
2	14.064	7.2	6.85	0.95	6.82	0.95
3	14.076	7.2	6.85	0.95	6.82	0.95
Average	14.171	7.2	6.85	0.95	6.82	0.95

1.   CD stands for characteristic distance.
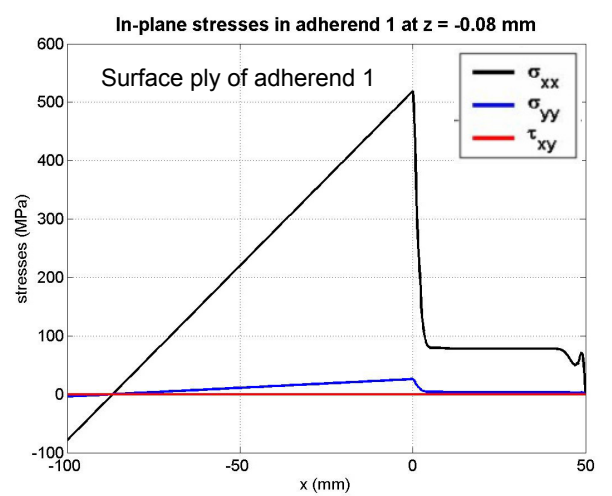2.   The ratio of the theoretical to the test results is based on the initial failure load.

Fig. 13 Through-thickness distribution of (a) margin of safety (MOS) of adherend 1 at point A1 and (b) in-plane stresses of the surface ply of adherend 1 with <u>linear</u> adhesive under P = 6.85 kN.
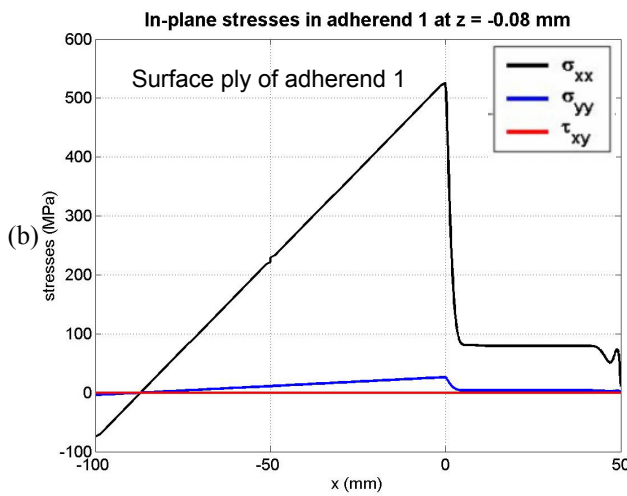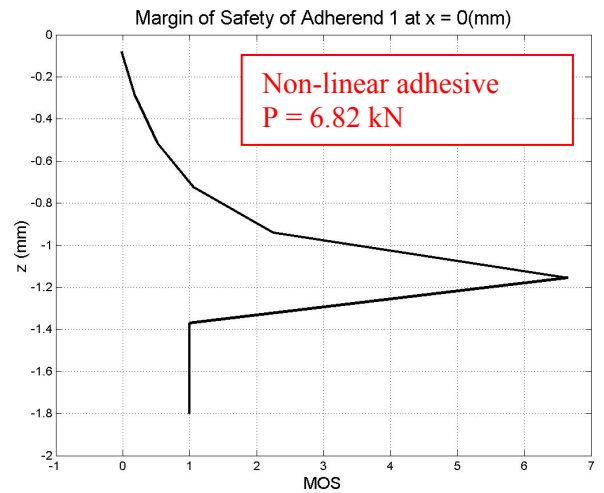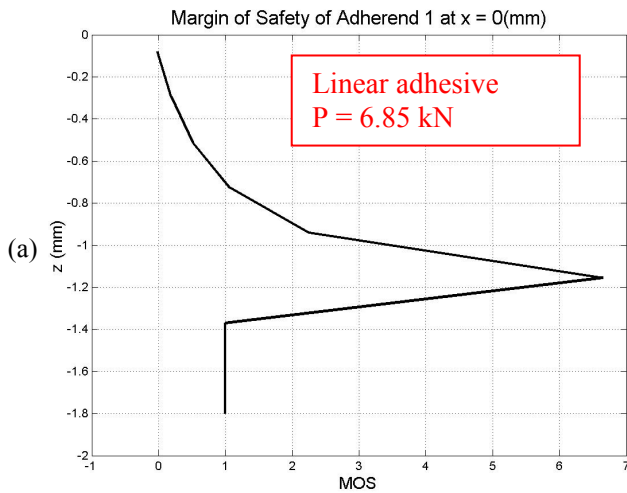
Fig.14 Through-thickness distribution of (a) margin of safety (MOS) of adherend 1 at point A1 and (b) in-plane stresses of the surface ply of adherend 1 with <u>nonlinear</u> adhesive under P = 6.82 kN.

V.   Discussion

Cheuk's bonded doubler problem shows that the failure location predicted by HyperSizer matches well with the experimental observation, while the predicted failure load with linear analysis is 13.5 kN, nonlinear result is 14.4 kN, both of which are reasonably accurate, but conservative, compared to the measured ultimate failure load in the tests, which is 18.6 kN. The discrepancy may be due to the progressive damage involved in the experiment and the predicted failure load by HyperSizer is only accounting for the damage initiation. Nonlinear analysis predicted a slightly higher failure load (14.4 kN), but it is still conservative compared to the test data. This is due to the section failure of the adherend being controlled by the in-plane tensile stress, which is less affected by the nonlinearity of the adhesive layer than the out-of-plane stresses.

In the NASA problem, the predicted location of damage onset by linear analysis is consistent with the experimental observation; and the predicted load for the damage initiation is approximately 0.76 times the

tested average strength of 17.8 kN. Nonlinear analysis shows that a more compliant adhesive will significantly increase the damage resistance of the adherend to matrix cracking and delamination, and HyperSizer predicts that the joint can carry 0.87 of the test failure load without failing. Davila[26], who also studied this problem, argued that matrix cracking should not be considered as the damage initiation mode because the initial matrix cracking is minor and soon turns into delamination. He suggested using delamination criteria for damage initiation, Eqs. (5) – (15) , instead of the one for matrix cracking.

The error between HyperSizer theoretical failure loads and the test results may also originate from the stress analysis. As observed in the comparison to FEA[1], the peak values of out-of-plane stresses predicted by HyperSizer are somewhat higher than finite element results. As such, HyperSizer's failure load predictions are generally on the conservative side, which is believed to be favorable to the preliminary design. In addition, to overcome the singularity problem encountered at free edges, we also used the characteristic distance in our failure analysis (NASA problem), where the stress analysis results should be more stable and accurate.

Another important issue that could cause the discrepancy between HyperSizer predicted results and test data is the boundary conditions used in the test articles. In solving for the stresses and displacements, HyperSizer makes the assumptions that these joints can only deform in "cylindrical bending", which states that deflections are a function of the panel y direction only. This means that deflections that vary in the x (or stiffener) direction, by panel curvature in that direction, are disallowed (see Fig. 15). These assumptions make it possible to solve for the stresses and strains in a very efficient manner compared to what would be required by solid finite element analysis. At first glance this might seem rather limiting, however, the question is: Does the cylindrical bending assumption limit the usefulness of this capability? We believe that for most real-world applications, this assumption, and therefore the HyperSizer methodology, is sufficient and appropriate.

Consider the typical skin-stringer structure shown in Fig. 15. In this situation, the stiffener to skin bonded joint is a part of what is referred to as an "in-service" panel. The panel is not isolated from other structures in the same way that a standalone test article would be. A panel in this situation is supported between stiff ringframes, bulkheads or ribs, which has two effects. First, the strain in the stiffener direction, ε_x, will be nearly constant throughout the panel. This is in contrast to the transverse strain ε_y which will be different between the panel facesheet and stiffener flange region. Second, because the effective bending stiffness of the panel is several orders of magnitude greater in the stiffener direction than in the transverse direction (i.e. $D_{11} \gg D_{22}$), the curvature in the stiffener direction will be much smaller than the curvature in the transverse direction. In fact, in most in-service loading conditions, the curvature in the stiffener direction can be assumed to be zero. In contrast to the in-service panel boundary condition is the case of a small, standalone test article, or even a transverse panel that is loaded in the transverse direction, but free to deform in the stiffener direction. This situation is depicted in Fig. 16. In this situation, unlike the in-service panel boundary condition, the panel is free to do several things that do not occur in actual aircraft panels. First, in the top view, it can be seen that the strain in both the x and y directions is non-uniform along the edges. Second, as seen in the side and front views, the panel may curve due to its eccentricity and the Poisson effect (this will cause the test article to deform in a saddle shape). Finally, because the individual plies each have primary stiffnesses in different directions, there is no guarantee that the edge will remain planar, and in fact could take on a stair step deformation as shown in the side view.

Modeling this type of stand-alone problem with greater accuracy would require a theory that does not assume cylindrical bending and models full 3-D elasticity for the individual plies. In general, this means using a 3-D solid model FEA. In addition, the HyperSizer methodology is intended for acreage panel structural problems and would not be expected to do as well in regions of panel closeouts or stiffener terminations. These types of problems would also require tests or detailed FEA. In summary, we expect even better correlation of HyperSizer with the majority of in-service aircraft structures.
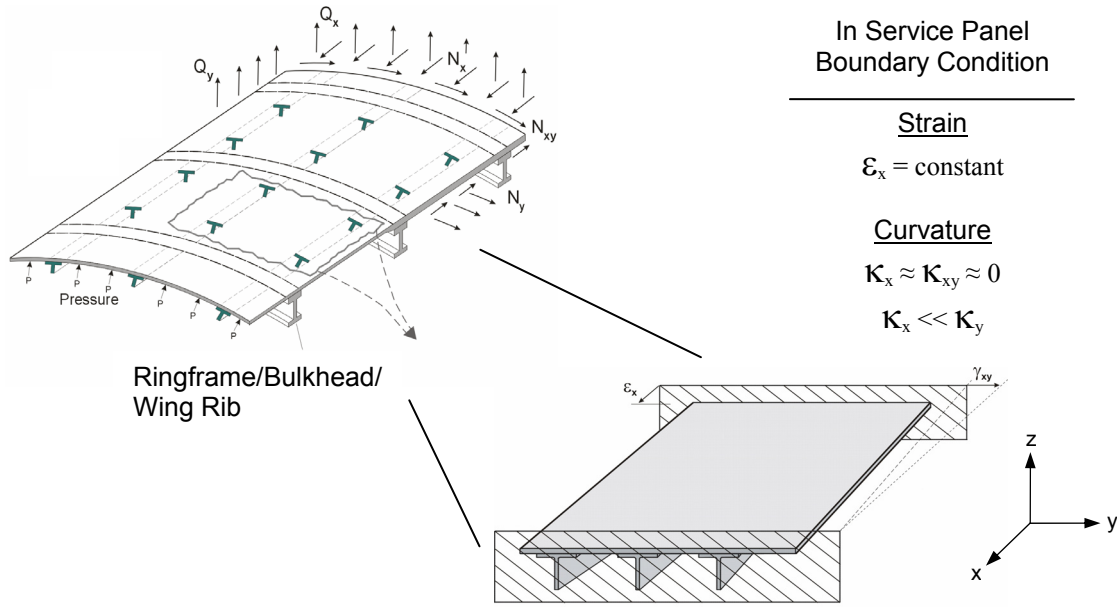
American Institute of Aeronautics and Astronautics

In Service Panel
Boundary Condition

Strain

$\varepsilon_x = $ constant

Curvature

$\kappa_x \approx \kappa_{xy} \approx 0$

$\kappa_x \ll \kappa_y$

Ringframe/Bulkhead/
Wing Rib

Fig. 15 The effective boundary conditions on an "in-service panel" enforce uniform edge deformation.

κ_x

Curvature due to
eccentricity and
Poisson's effect

Stair step strain of
individual plies

ε_y, **non-uniform**
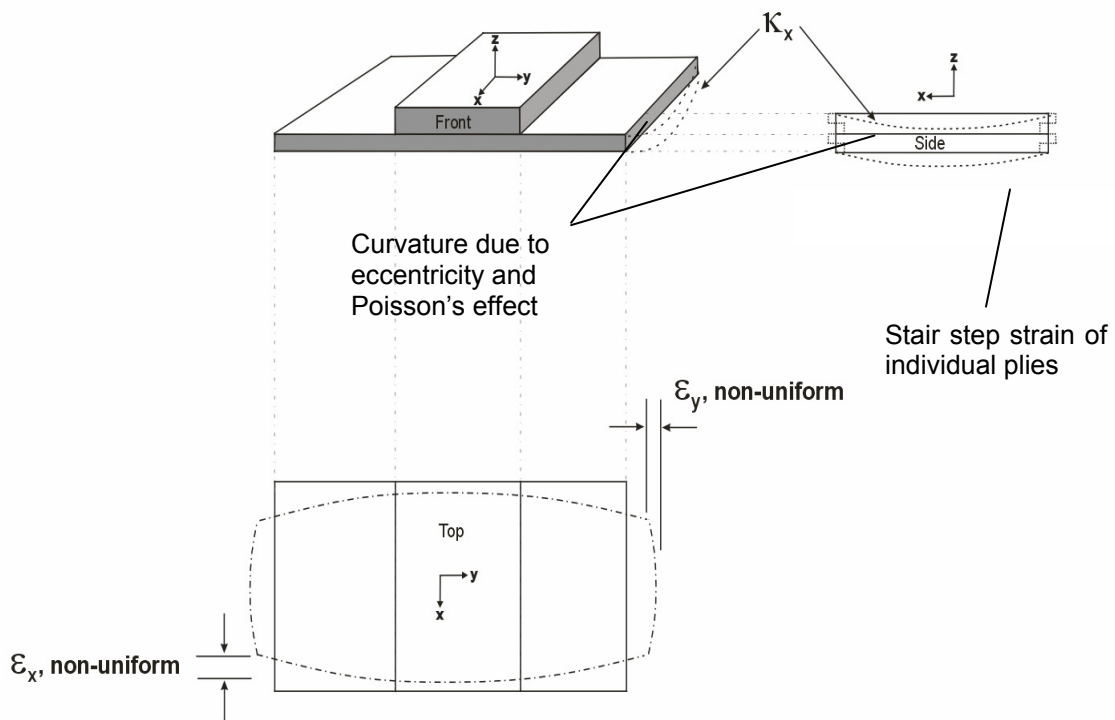
ε_x, **non-uniform**

Fig. 16 Free boundary conditions on standalone test article permit non-uniform edge deformation and curvature in both axes.

VI. Conclusion

A method for stress analysis of composite bonded joints was recently developed and implemented in a new capability called HyperSizer. Together with suitable failure criteria, summarized in this paper, HyperSizer can predict the failure of composite joints. Three joint configuration designs were selected from the literature for validation: Cheuk's[2] bonded doubler problem, NASA's[3] skin/stepped flange problem, and Tong's[6] single-lap joint problem. The ratios of theoretical failure divided by test average failure for the total of 14 test cases vary from 0.77 to 0.95, with average of 0.86. Table 8 summarizes the theoretical failure loads and test averages together with failure criteria used in the analysis. These results show that HyperSizer is relatively accurate and consistent at predicting initial failure.

Table 8 Summary of theoretical predictions vs. test averages

			Test example 1 Bonded doubler by Cheuk		Test example 2 Bonded doubler by NASA		Test example 3 Single-lap joints by Tong	
			Theoretical Failure Load (kN)	Ratio of the Theoretical to the Test	Theoretical Failure Load (kN)	Ratio of the Theoretical to the Test	Theoretical Failure Load (kN)	Ratio of the Theoretical to the Test
HyperSizer	Linear Adhesive	CD* = 0	13.5	0.73	12.3	0.69	6.85	0.95
		CD = ½ t $_{ply}$	N/A	N/A	13.5	0.76	N/A	N/A
	Nonlinear Adhesive	CD = 0	14.4	0.77	13.9	0.78	6.82	0.95
		CD = ½ t $_{ply}$	N/A	N/A	15.4	0.87	N/A	N/A
	Failure Modes and Criterion Used		Sectional fracture: Max principal stress, i.e., Eq. (17)		Delamination: Eq. (13) Matrix cracking: Eq. (16)		First ply fracture: Max in-plane stress, i.e., Eq. (17)	
Test	Damage Initiation Load (kN)		N/A		average = 17.8		average = 7.2	
	Ultimate Failure Load (kN)		average = 18.6		N/A		average = 14.2	

*CD stands for characteristic distance.

References

[1]Zhang, J., Bednarcyk, B., Collier, C., Yarrington, P., and Bansal, Y., and Pindera, M.-J., "3D Stress Analysis of Composite Bonded Joints," Proc. The 46th AIAA/ASME/ASCE/AHS/ASC Structures, Structural Dynamics, and Materials Conference, April, 2005, Austin, Texas.

[2]Cheuk, P.T. and Tong L., "Failure of Adhesive Bonded Composite Lap Shear Joints with Embedded Precrack," *Composites Science and Technology*, Vol. 62, 2002, pp.1079-1095.

[3]Krueger, R., Paris, I. L., O'Brien T. K., and Minguet, P. J., "Fatigue Life Methodology for Bonded Composite Skin/Stringer Configurations," NASA/TM-2001-210842, ARL-TR-2432, 2001.

[4]Krueger, R., Paris, I. L., O'Brien T. K., and Minguet, P. J., "Testing and Analysis of Composite Skin/Stringer Debonding under Multi-axial Loading," *Journal of Composite Materials*, Vol. 34, 2000, pp. 1263-1300.

[5]Krueger, R., Paris, I. L. and O'Brien, T. K., 2000, "Fatigue Life Methodology for Bonded Composite Skin/Stringer Configurations," Proc. The American Society for Composites, 15th Technical Conference, pp. 729-736.

[6]Tong, L., "Failure of Adhesive-Bonded Composite Single Lap Joints with Embedded Cracks," *AIAA Journal*, Vol. 36, No. 3, 1998, pp. 448-456.

[7]Mortensen, F. and Thomsen, O.T., "Analysis of Adhesive Bonded Joints: A Unified Approach," *Composites Science and Technology*, Vol. 62, 2002, pp. 1011-1031.

[8]Hashin, Z., and Rotem, A., "A Fatigue Criterion for Fiber-Reinforced Materials," *Journal of Composite Materials*, Vol. 7, 1973, pp. 448-464.

[9]Hashin, Z., "Failure Criteria for Unidirectional Fiber Composites," *Journal of Applied Mechanics*, Vol. 47, 1980, pp. 329-334.

[10]Sun C.T., Tao J.X., "Prediction of Failure Envelopes and Stress Strain Behaviors of Composite Laminates," *Composites Science and Technology*, Vol. 58, 1998, pp. 1125–1136.

[11]Puck, A., Kopp J., and Knops M., "Guidelines for the Determination of the Parameters in Puck's Action Plane Strength Criterion," *Composites Science and Technology*, Vol. 62, 2002, pp. 371–378.

[12]Davila, C.G. and Camanho, P.P., "Failure Criteria for FRP Laminates in Plane Stress," NASA/TM-2003-212663.

[13]Heslehurst, R. B. and Hart-Smith, L., "The Science and Art of Structural Adhesive Bonding," SAMPE Journal, Vol. 38, 2002, pp. 60-71.

[14]Adams, R.D. and Wake, W.C., Structural Adhesive Joints in Engineering. London: Elsevier Applied Science Publishers, 1984.

[15]Hoyt, D.M., Ward, S.H., Minguet, P.J., "Strength and Fatigue Life Modeling of Bonded Joints in Composite Structure," Proc. American Society for Composites (ASC) 15th Technical Conference, September 2000.

[16]Long R.S., "Static Strength of Adhesively Bonded ARALL-1 Joints," *Journal of Composite Materials*, Vol. 25, 1991, pp. 391-415.

[17]Tong, L., "An Assessment of Failure Criteria to Predict the Strength of Adhesively Bonded Composite Doubler Lap Joints," *Journal of Reinforced Plastics and Composites*, Vol. 16, No. 18, 1997, pp. 698-713.

[18]Camanho, P.P. and Matthews, F.L., "Delamination Onset Prediction in Mechanically Fastened Joints in Composite Laminates," *Journal of Composite Materials*, Vol. 33, No. 10, 1999, pp. 906-927.

[19]Minguet, P.J., Fedro, M.J., O'Brien, T.K., Martin, R.H. and Ilcewicz, L.B., "Development of a Structural Test Simulating Pressure Pillowing Effects in Bonded Skin/Stringer/Frame Configuration," Proc. The Fourth NASA/DoD Advanced Composite Technology Conference, Salt Lake City, Utah, 1993.

[20]Minguet, P.J. and O'Brien, T.K., "Analysis of Test Methods for Characterizing Skin/Stringer Debonding Failures in Reinforced Composite Panels," in Composite Materials: Testing and Design (Twelfth Volume), ASTM STP 1274, 1996, pp. 105-124.

[21]Minguet, P.J. and O'Brien, T.K., "Analysis of Composite Skin/Stringer Bond Failures Using a Strain Energy Release Rate Approach," Proc. The Tenth International Conference on Composite Materials, Vol. I, A. Poursartip and K. Street, Eds., 1995, pp. 245-252.

[22]Minguet, P.J., "Analysis of the Strength of the Interface Between Frame and Skin in a Bonded Composite Fuselage Panel," Proc. The AIAA/ASME/ASCE/AHS/ASC Structures, Structural Dynamics and Materials Conference, 1997, pp. 2783-2790.

[23]Adams, R. and Harris, J.A., "The Influence of Local Geometry on the Strength of Adhesive Joints," *International Journal of Adhesion and Adhesives*, Vol. 7, No. 2, 1987, pp. 69-80.

[24]Adams, R.D. and Peppiatt, N.A, "Stress Analysis of Adhesive-Bonded Lap Joints," *Journal of Strain Analysis*, Vol. 9, No. 3, 1974, pp. 185-196.

[25]Collier Research Corp., "Consistent Structural Integrity and Efficient Certification with Analysis," AF SBIR report F33615-02-C-3216, Vol. 1-3, 2004.

[26]Davila, C., Personal Communication.

[27]Tong, L. and Steven, G.P., Analysis and Design of Structural Bonded Joints, Kluwer Academic Publishers, 1999.

[28]Tsai, M.Y., Morton, J, and Matthews, F.L., "Experimental and Numerical Studies of a Laminated Composite Single-Lap Adhesive Joint" *Journal of Composite Materials*, Vol. 29, No. 9, 1995, pp.1254-1275.